No.336 (#9 – 15)

9. **Aluminum-26 Enrichment in the Surface of Protostellar Disks Due to Protostellar Cosmic Rays**
10. Chamaeleon DANCe. Revisiting the stellar populations of Chamaeleon I and Chamaeleon II with Gaia-DR2 data
11. **ALMA chemical survey of disk-outflow sources in Taurus (ALMA-DOT) V: Sample, overview, and demography of disk molecular emission**
12. The Geometry and Dynamical Role of Stellar Wind Bubbles in Photoionised HII Regions
13. 3D dynamics of the Orion cloud complex Discovery of coherent radial gas motions at the 100-pc scale
14. Simulating Star Clusters Across Cosmic Time: II. Escape Fraction of Ionizing Photons from Molecular Clouds
15. Water maser variability in a high-mass YSO outburst - VERA and ALMA observations of S255 NIRS 3

#9「原始星表面からの宇宙線による原始惑星系円盤表面での^{26}Al濃縮」

^{26}Al Enrichment in the Surface of Protostellar Disks Due to Protostellar Cosmic Rays

Brandt A. L. Gaches, Stefanie Walch, Stella S. R. Walch, Carsten Münker

The radioactive decay of aluminum-26 (^{26}Al) is an important heating source in early planet formation. Since its discovery, there have been several mechanisms proposed to introduce ^{26}Al into protoplanetary disks, primarily through contamination by external sources. We propose a local mechanism to enrich protostellar disks with ^{26}Al through irradiation of the protostellar disk surface by cosmic rays accelerated in the protostellar accretion shock. We calculate the ^{26}Al enrichment, $[^{26}\mathrm{Al}/^{27}\mathrm{Al}]$, at the surface of the protostellar disk in the inner AU throughout the evolution of low-mass stars, from M-dwarfs to proto-Suns. Assuming constant mass accretion rates, $\dot{m}$, we find that irradiation by MeV cosmic rays can provide significant enrichment on the disk surface if the cosmic rays are not completely coupled to the gas in the accretion flow. Importantly, we find that low accretion rates, $\dot{m} < 10^{-7}$ $\mathrm{M_\odot\ yr^{-1}}$, are able to produce canonical amounts of ^{26}Al, $[^{26}\mathrm{Al}/^{27}\mathrm{Al}] \approx 5 \times 10^{-5}$. These accretion rates are experienced at the transition from Class I- to Class II-type protostars, when it is assumed that calcium-aluminum-rich inclusions condense in the inner disk. We conclude that irradiation of the inner disk surface by cosmic ray protons accelerated in accretion shocks at the protostellar surface may be an important mechanism to produce ^{26}Al. Our models show protostellar cosmic rays may be a viable model to explain the enrichment of ^{26}Al found in the Solar System.

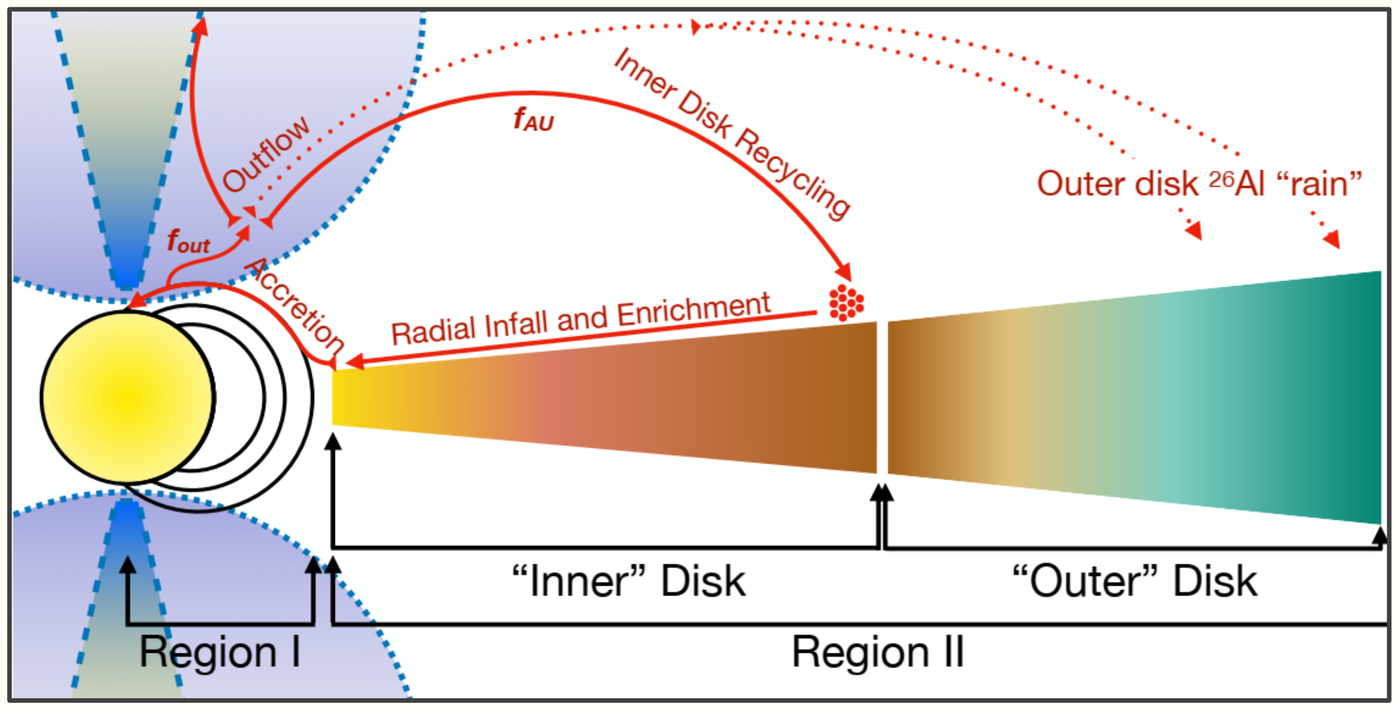

- calcium-aluminum-rich inclusions (CAIs) での標準的な値 $[^{26}\mathrm{Al}/^{27}\mathrm{Al}]$ = 5e-5が分かっている。これは銀河系での平均よりも高い。
- またChondruleでは最大一桁小さい。これは太陽系の領域によって^{26}Alの組成が異なる可能性を示唆する。
- ^{26}Alの半減期は短い (0.717[Myr]) ため、原始太陽の原始惑星系円盤での^{26}Alの生成・混合が必要となる。

目的：^{26}Alの濃縮機構の解明

外部起源シナリオ

A) 近傍の超新星残骸からのガス (Cameron & Truan 1977)
B) 星風 (e.g., Gounelle & Meynet 2012)

- 外部起源シナリオには２つ弱点がある
  1. 限定された環境パラメータを要求する (星質量、分子雲との距離、ガスの注入速度・密度)
  2. (あり得ないほど)短時間での注入ガスと原始惑星系ガスの混合が必要

local sourceシナリオ

- ダストグレイン凝縮より先に、^{26}Alをディスクに直接注入できるため、混合時間の問題をクリア

A) Tタウリ星のフレア活動中に生成される宇宙線 (Lee et al. 1998) → 予想される^{26}Al組成が太陽系の値に比べて低い
B) 新たなメカニズム：Class I/II期の原始惑星系円盤表面に、若い原始星への降着衝撃波で加速された宇宙線からの陽子が照射されることによる濃縮

モデル：降着中の原始星周りの定常円盤

- ディスク中のガスは内側へと流れる
- 宇宙線は降着衝撃波中で加速される。円盤に照射して^{26}Alを増やす
- 降着ガスの一部 (f_{out}=0.1) はアウトフローに取り込まれる。さらにその一部 (f_{AU}=0.1) は内部円盤に戻る。

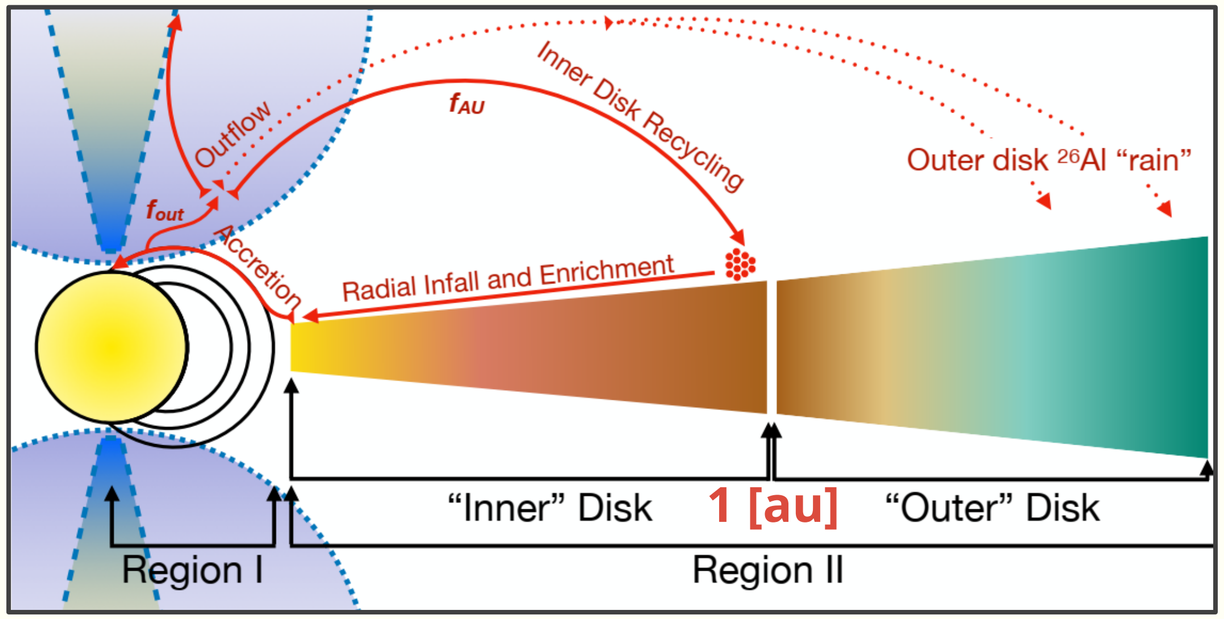

初期条件：n(^{26}Al)/n(^{27}Al) = 0 at R = 1 [au]

- １次元円盤プロファイル：
- 降着速度：
- 降着率 (モデル・パラメータ)：
- ^{26}Alの増加：

$$\Sigma(r) = \Sigma_0 \left(\frac{r}{r_0}\right)^{-p} \quad T(r) = T_0 \left(\frac{r}{r_0}\right)^{-q}$$

$$v_r = \dot{m}/(2\pi r \Sigma(r))$$

$$\dot{m} = (10^{-9}, 10^{-8}, 10^{-7} \text{ and } 10^{-6}) \ \mathrm{M}_\odot \ \mathrm{yr}^{-1}$$

$$f(^{26}\mathrm{Al})_{i+1} = f_{\mathrm{AU}} f_{\mathrm{out}} \left(\frac{n_i(^{26}\mathrm{Al})}{n_i(^{27}\mathrm{Al})}\right)$$
$$n_{i+1}(^{26}\mathrm{Al}) = f(^{26}\mathrm{Al})_{i+1} X(\mathrm{Al}) n_{\mathrm{H}}$$
$$n_{i+1}(^{27}\mathrm{Al}) = (1 - f(^{26}\mathrm{Al})_{i+1}) X_{\mathrm{Al}} n_{\mathrm{H}}.$$

終了条件：原始星質量 m_* = 0.05 → 2 [$M_\odot$]

中心星からの距離に依存する宇宙線スペクトル f(E, r) を計算

円盤表面での^{26}Alの生成率を計算：

$$\zeta(i) = \int_{E_{th}}^{\infty} f(E)\sigma_i(E)dE,$$

- 陽子との反応３種を取り扱う：

$$^{27}\mathrm{Al} + p \rightarrow ^{26}\mathrm{Al} + \mathrm{pn},$$

- 反応率はテーブルを用いる。

$$^{26}\mathrm{Mg} + p \rightarrow ^{26}\mathrm{Al} + \mathrm{n},$$

$$^{28}\mathrm{Si} + p \rightarrow ^{26}\mathrm{Al} + ^{3}\mathrm{He}$$

^{26}Al・^{27}Alの同位体組成計算

$$\frac{dn(^{26}\mathrm{Al})}{dt} = n(^{27}\mathrm{Al})\zeta(^{27}\mathrm{Al}) + n(^{26}\mathrm{Mg})\zeta(^{26}\mathrm{Mg}) + n(^{28}\mathrm{Si})\zeta(^{28}\mathrm{Si}) - \frac{n(^{26}\mathrm{Al})}{\tau_{^{26}\mathrm{Al}}}$$

$$\frac{dn(^{27}\mathrm{Al})}{dt} = -n(^{27}\mathrm{Al})\zeta(^{27}\mathrm{Al})$$

$$\frac{dn(^{26}\mathrm{Mg})}{dt} = -n(^{26}\mathrm{Mg})\zeta(^{26}\mathrm{Mg}) + \frac{n(^{26}\mathrm{Al})}{\tau_{^{26}\mathrm{Al}}}$$

$$\frac{dn(^{28}\mathrm{Si})}{dt} = -n(^{28}\mathrm{Si})\zeta(^{28}\mathrm{Si}).$$

- 初期組成には太陽組成を採用する。

Model #	Description
1	Fiducial
2	$\mathrm{B}_* = 10^1$ G
3	$\varepsilon = 10^{-3}$
4	$f_{\mathrm{tot}} = 0.25$

(B$_*$=10^{3}G, ε=0.1, f$_{out}$=0.1)

：原始星の磁場強度

：宇宙線とガスの結合係数

：= f$_{AU}$×f$_{out}$

注意：下図中の線が赤いほど低降着率・青いほど高降着率

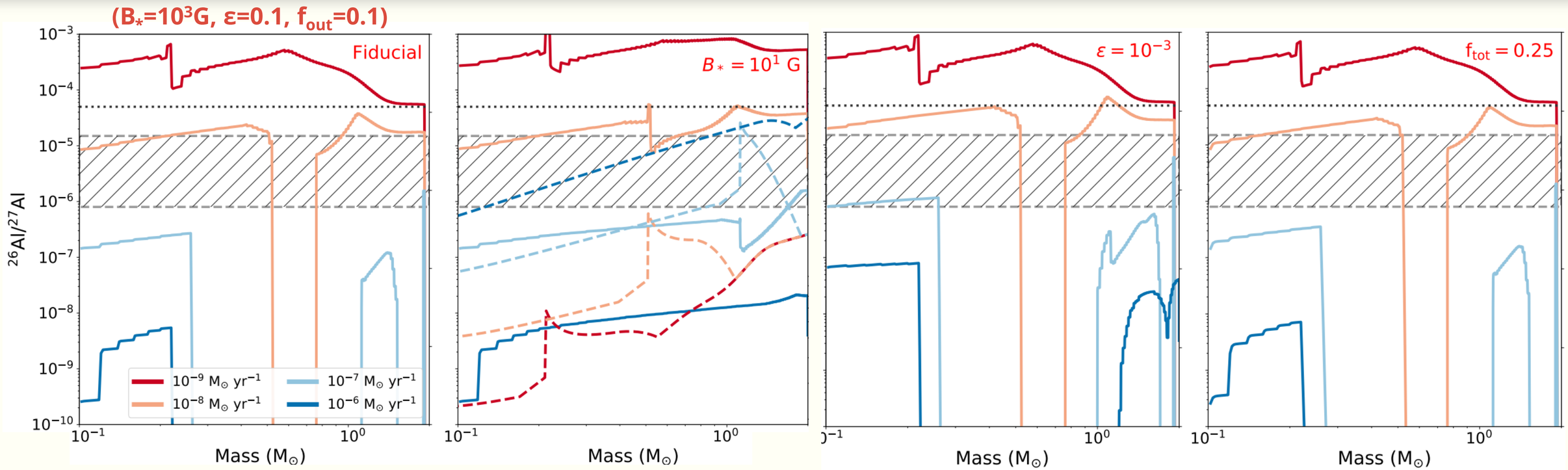

$^{26}Al/^{27}Al$の時間進化 (原始星質量 = 0.05 → 2 [$M_\odot$])

- 比較的低い降着率でも十分な^{26}Al組成が実現 (高降着率の場合、衝撃波の柱密度と原始星半径が増大してしまうため、^{26}Al生成を阻害する)
- 特に円盤の内側では、低降着率 (<1e7[$M_\odot$/yr])でも十分な^{26}Al組成が作られた。この降着率は、低質量原始星がClass IからII天体へと遷移する段階の降着率に近い。

(1)原始星の磁場強度と(2)原始星半径が^{26}Al生成を左右する

#9 Results & Discussion

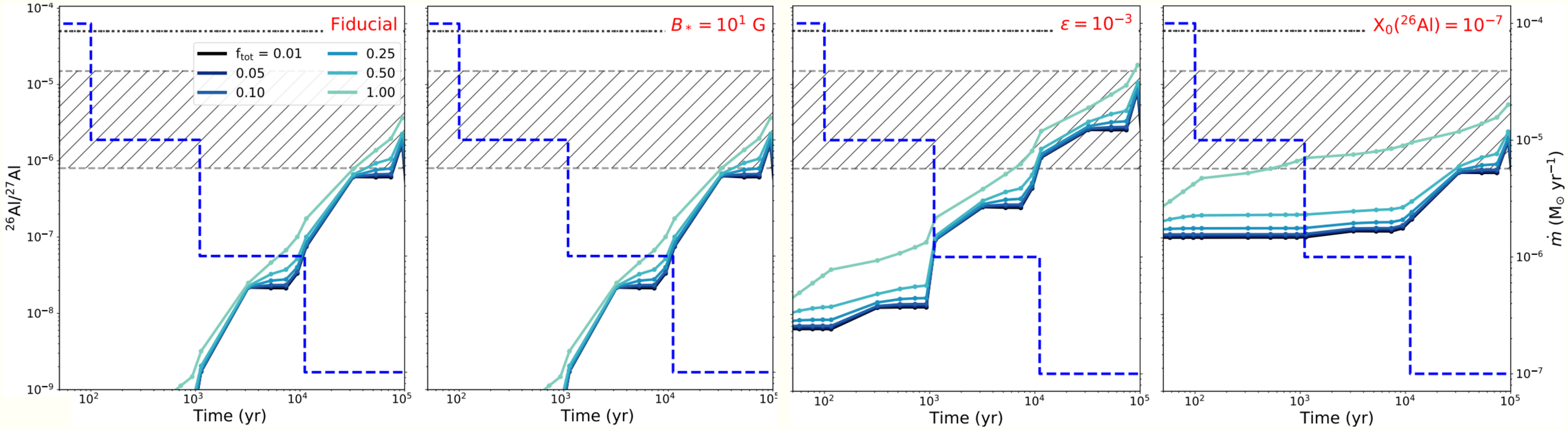

実際には、原始星への降着率は時間と共に減少する。簡単な階段関数 (上図の青破線) を使って影響を調べた。

- 降着率がある程度低くなった時に^{26}Al生成が進む。
- ^{26}Al/^{27}Alは、全てのモデルでChondriteで測定された値まで増加した。
- εが低いモデルの円盤内側でのみ、隕石での標準値 (^{26}Al/^{27}Al =5e-5) まで増加した。

ALMA chemical survey of disk-outflow sources in Taurus (ALMA-DOT) V: Sample, overview, and demography of disk molecular emission

Antonio Garufi, Linda Podio, Claudio Codella, Davide Fedele, Eleonora Bianchi, Cecile Favre, Francesca Bacciotti, Cecilia Ceccarelli, Seyma Mercimek, Kazi Rygl, Richard Teague, Leonardo Testi We present an overview of the ALMA chemical survey of disk-outflow sources in Taurus (ALMA-DOT), a campaign devoted to the characterization of the molecular emission from partly embedded, young stars. The project aims at better understanding the gaseous products that are delivered to planets by means of high-resolution maps of assorted lines probing disks at the time of the planet formation (less than 1 Myr). Nine different molecules are surveyed by our observations of six Class I/flat-spectrum sources. A series of accompanying articles analyze specific targets and molecules. Here we describe the sample and provide a general overview of the results, focusing on the spatial distribution, column densities, and abundance ratios of H_2CO, CS, and CN. The results of this work are a first step toward the characterization of the disk chemical evolution that need to be complemented by further observations of less exceptional disks and customized thermo-chemical modeling.

ALMA-DOT (Disk-Outflow sources in Taurus)

- ターゲット：６つのClass I天体
- 観測：ALMA Cycle 4 & 6
- 輝線：９種 (本稿では内７種に触れる)

Table 1. Stellar properties of all targets in the ALMA-DOT program.

Target	SpT	Mass ($M_\odot$)	d (pc)	Ref.
DG Tau	K7	0.3	121.2	a, 1
DG Tau B	-	1.1	140	b, 2
HL Tau	K3	2.1	147.3	c, 3
Haro 6-13	K5	1.0	130.4	d, 1
IRAS 04302+2247	-	2.0	161	e, 4
T Tau N, Sa, Sb	K0, -, M	2, 2, 0.5	144.3	f, 1

Paper 0-III：特定天体に注目

Paper IV, VI：特定分子の注目

Paper V：全サンプルを用いた(特に)H2CO, CS, CNの解析 (統計的議論)

#11 各天体の観測結果

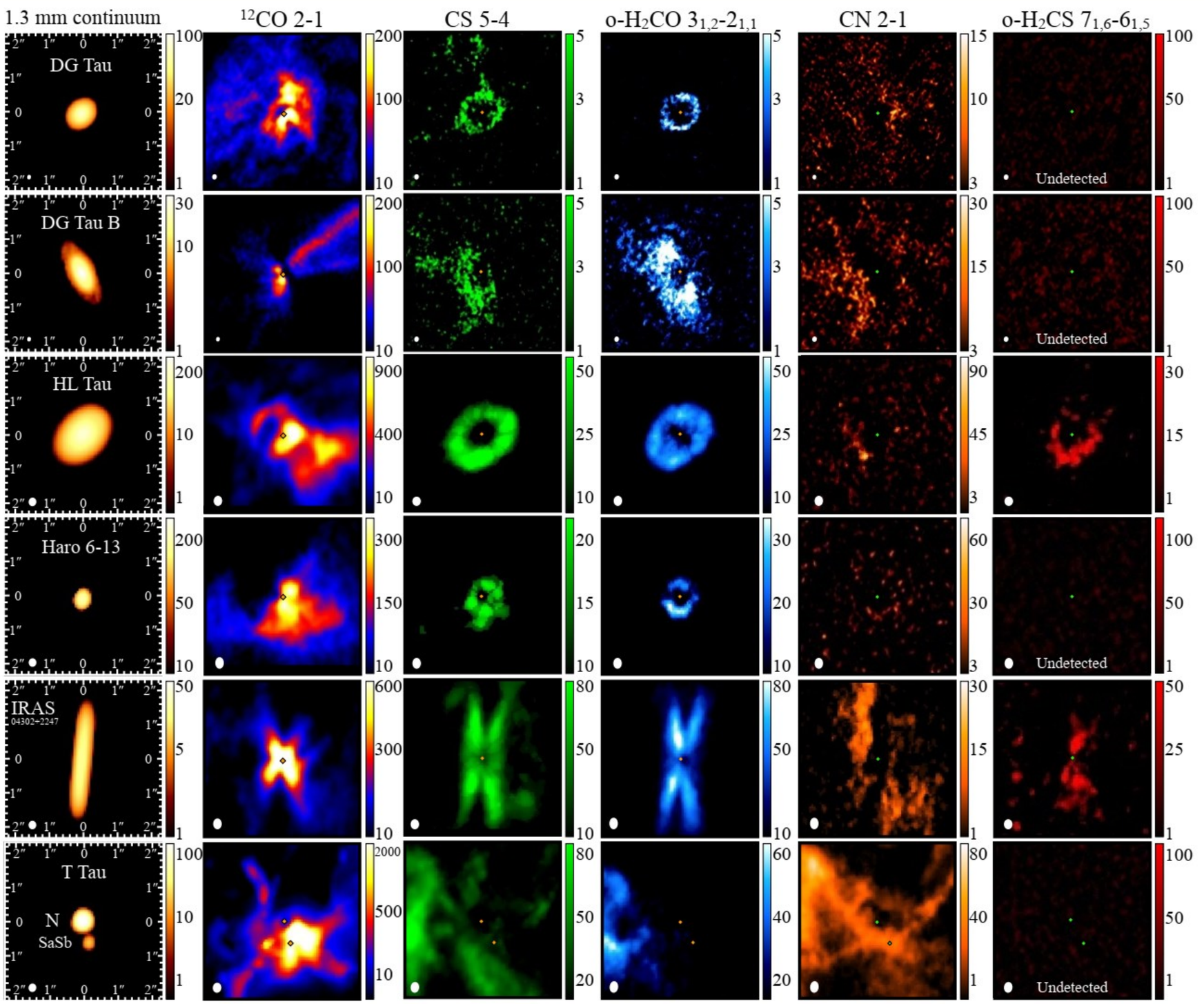

Table 2. Molecular lines probed by the ALMA-DOT campaign and analyzed in this work. The available dataset also includes several lines of SO and SO_2 that are described in a forthcoming work.

Molecule	Transition	ν_{rest} (GHz)	E_{up} (K)	$S_{ij}\mu^2$ (D^2)
^{12}CO	2–1	230.53800	17	0.02
o-H_2CO	$3_{1,2} - 2_{1,1}$	225.69777	33	43.5
CS	5–4	244.93555	35	19.1
CN	2–1, $\frac{3}{2} - \frac{1}{2}, \frac{3}{2} - \frac{3}{2}$	226.63219	16	1.2
	2–1, $\frac{3}{2} - \frac{1}{2}, \frac{5}{2} - \frac{3}{2}$	226.65956	16	4.2
	2–1, $\frac{3}{2} - \frac{1}{2}, \frac{1}{2} - \frac{1}{2}$	226.66369[b]	16	1.2
	2–1, $\frac{3}{2} - \frac{1}{2}, \frac{3}{2} - \frac{1}{2}$	226.67931	16	1.6
	2–1, $\frac{5}{2} - \frac{3}{2}, \frac{7}{2} - \frac{5}{2}$	226.87478	16	6.7
	2–1, $\frac{5}{2} - \frac{3}{2}, \frac{5}{2} - \frac{3}{2}$	226.87419[b]	16	4.2
	2–1, $\frac{5}{2} - \frac{3}{2}, \frac{3}{2} - \frac{1}{2}$	226.87589[b]	16	2.6
	2–1, $\frac{5}{2} - \frac{3}{2}, \frac{3}{2} - \frac{3}{2}$	226.88742	16	0.8
	2–1, $\frac{5}{2} - \frac{3}{2}, \frac{5}{2} - \frac{5}{2}$	226.89212	16	0.8
HDO	$3_{1,2} - 2_{2,1}$	225.89672	168	0.7
	$2_{1,1} - 2_{1,2}$	241.56155	95	0.4
CH_3OH	$3_{-2,2} - 4_{-1,4}$ (E)	230.02706	40	2.9
	$5_{0,5} - 4_{0,4}$ (A)	241.79143	35	16.2
o-H_2CS	$7_{1,6} - 6_{1,5}$	244.04850	60	55.9

CO：円盤以外の成分が混ざる。

CS, H2CO：円盤によく対応。

CN：円盤の外領域に対応。

H2CS：２天体で検出。円盤に対応。

CH3OH：１天体のみ検出。

HDO：全天体で未検出。

#11 PV図

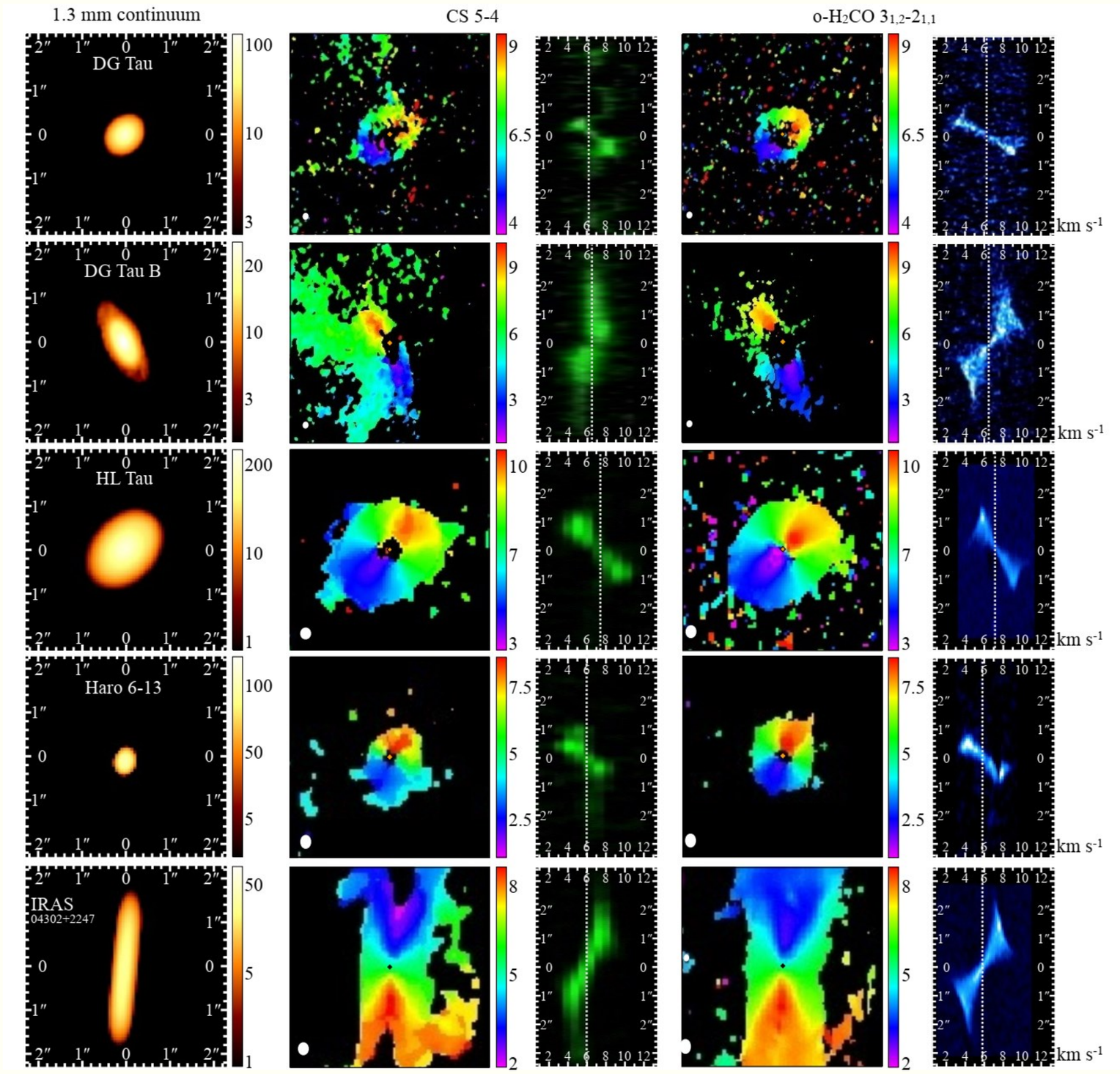

CS, H2COは円盤からの強く放射しており、円盤の運動構造を確認できる(PV図)。

H2COの方が円盤をよく表す。

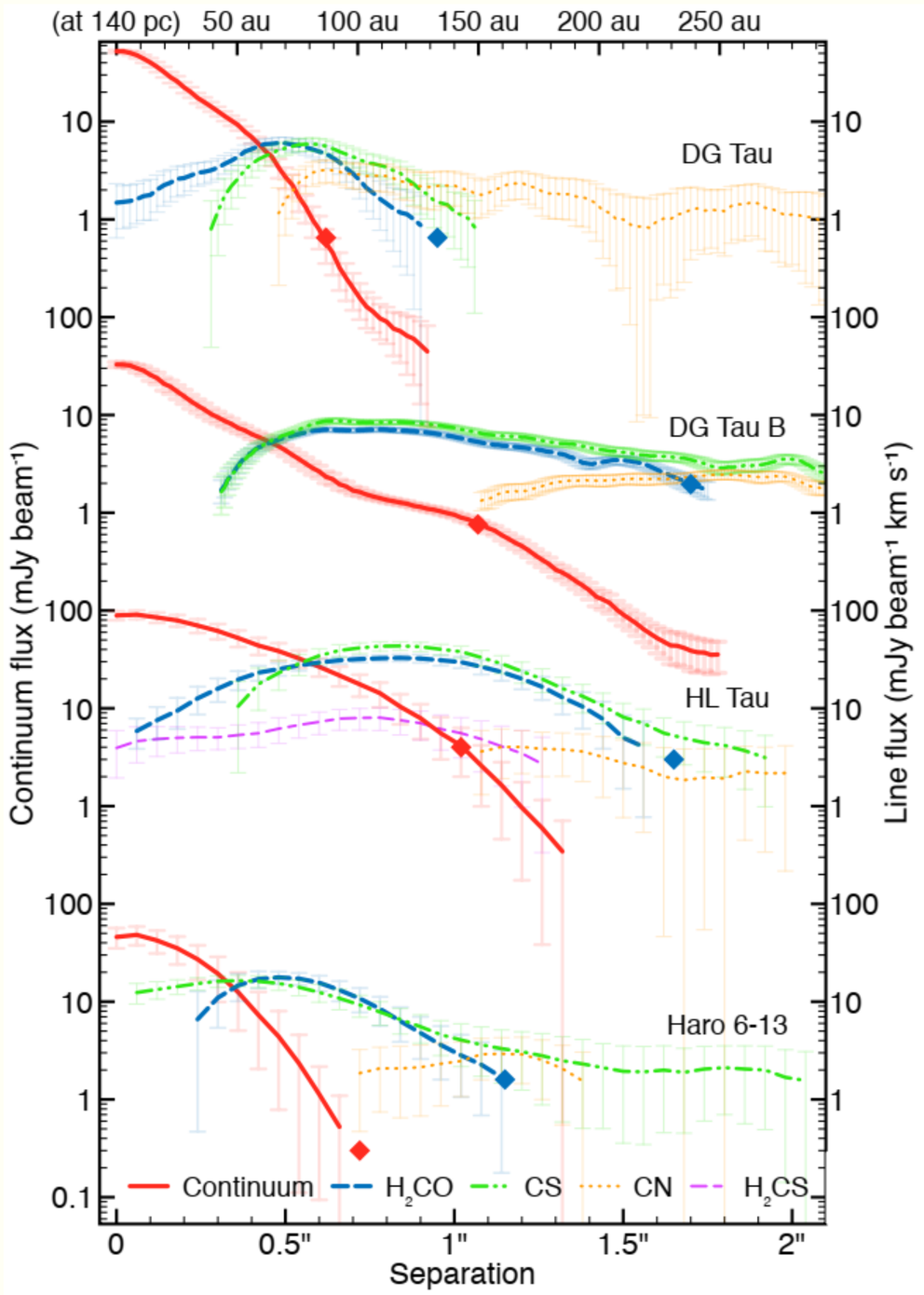

Fig. 3. Radial profile of the continuum and spectral line emission, ob-

Table 3. Properties of dust and H_2CO emission.

Target	P.A. (°)	i (°)	z/r	$r_{out,d}$ (au)	$r_{in,g}$ (au)	$r_{out,g}$	δr_{out}
DG Tau	135	35	0.09	75	35	120	1.6
DG Tau B	24	62	0.21	150	45	240	1.6
HL Tau	138	47	0.16	150	55	250	1.7
Haro 6-13	167	38	0.07	100	30	150	1.5
IRAS 04302	175	81	0.23	240	50	390	1.6

Notes. Columns: target name, disk position angle, inclination, opening angle, outer radius of the dust emission, inner and outer radius of the gas emission, and ratio between the dust and gas outer radii.

radial profileより

・ガス(輝線)はダスト(連続光)より外に広がっている。

・半径は天体によって異なるが、ダストとガス(H2CO)の半径比率 δr_{out} ~ 1.6 は天体間で大きな差がない。

・他の天体 (θ~0.3″) に比べて高分解能観測 (θ~0.15″)を行ったDG Tau・DG Tau Bにはダストのサブ構造が見られる。

・円盤中心では全ての輝線フラックスが減少している。

#11 各輝線の柱密度

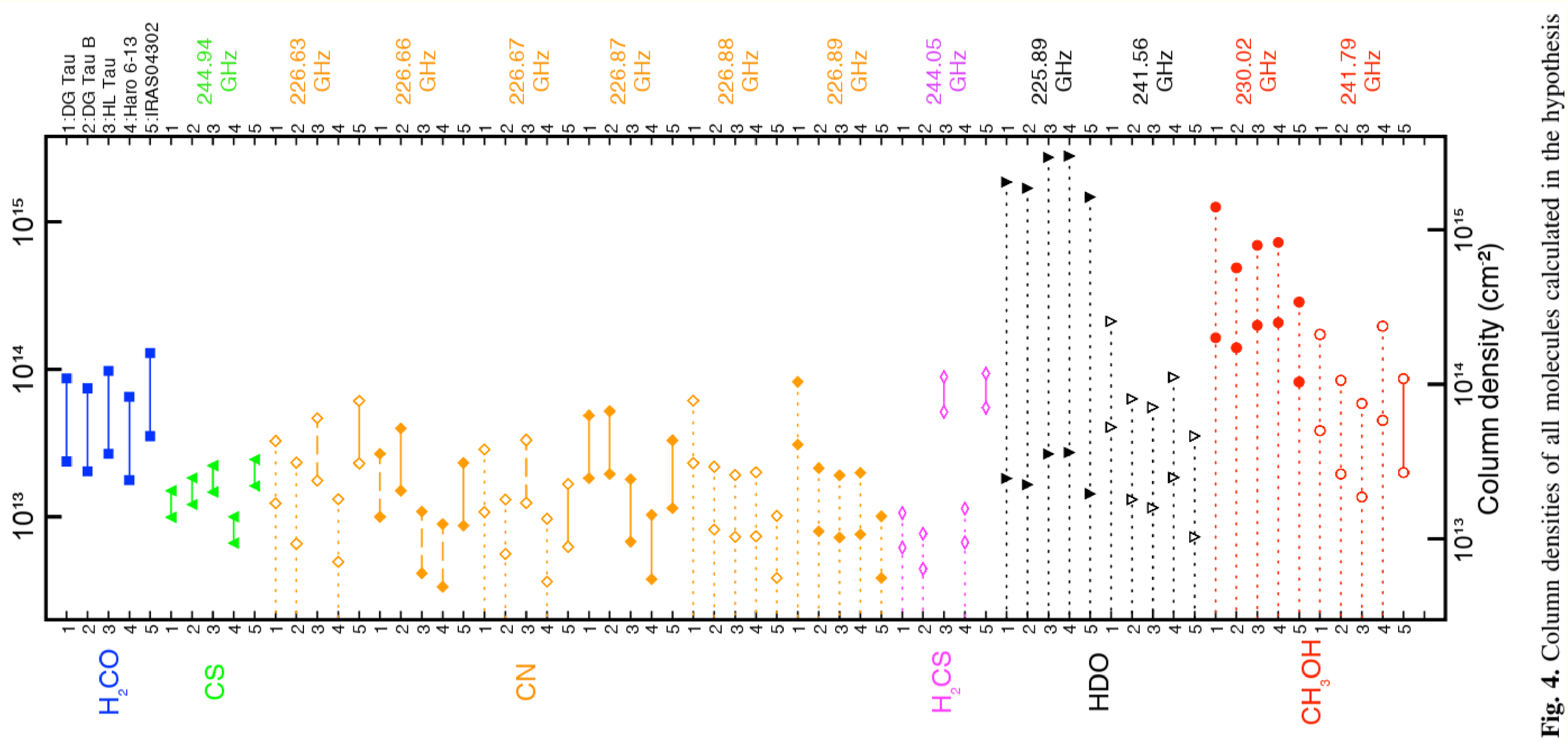

Fig. 4. Column densities of all molecules calculated in the hypothesis

「光学的に薄く」「局所熱平衡(LTE)」が成り立つと仮定し、各輝線の光度を柱密度に変換した。

・ガス温度を最小値 – 最大値 = 20 – 100[K] とし、柱密度の範囲を計算している。

#11 柱密度・柱密度比

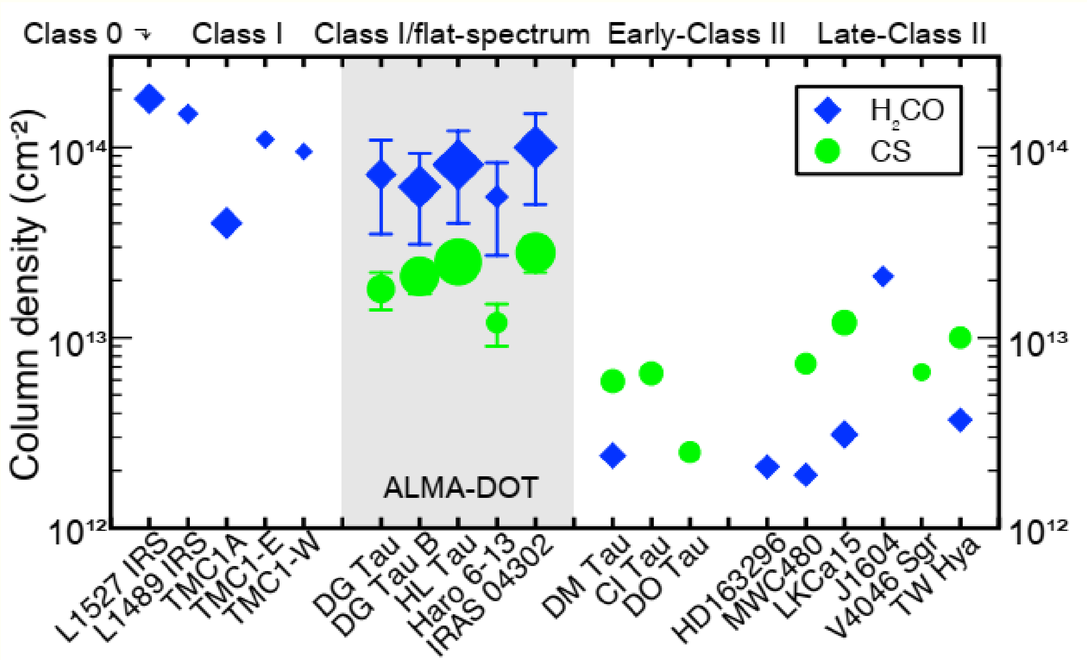

Fig. 6. CS and H_2CO column densities from this work compared with

H2CO・CSの柱密度を他の文献と比較

・柱密度は、原始星の進化と共に低下する傾向にある

・H2CO・CSの大小関係が逆転している (円盤における化学組成進化が異なる？)

重要な柱密度比

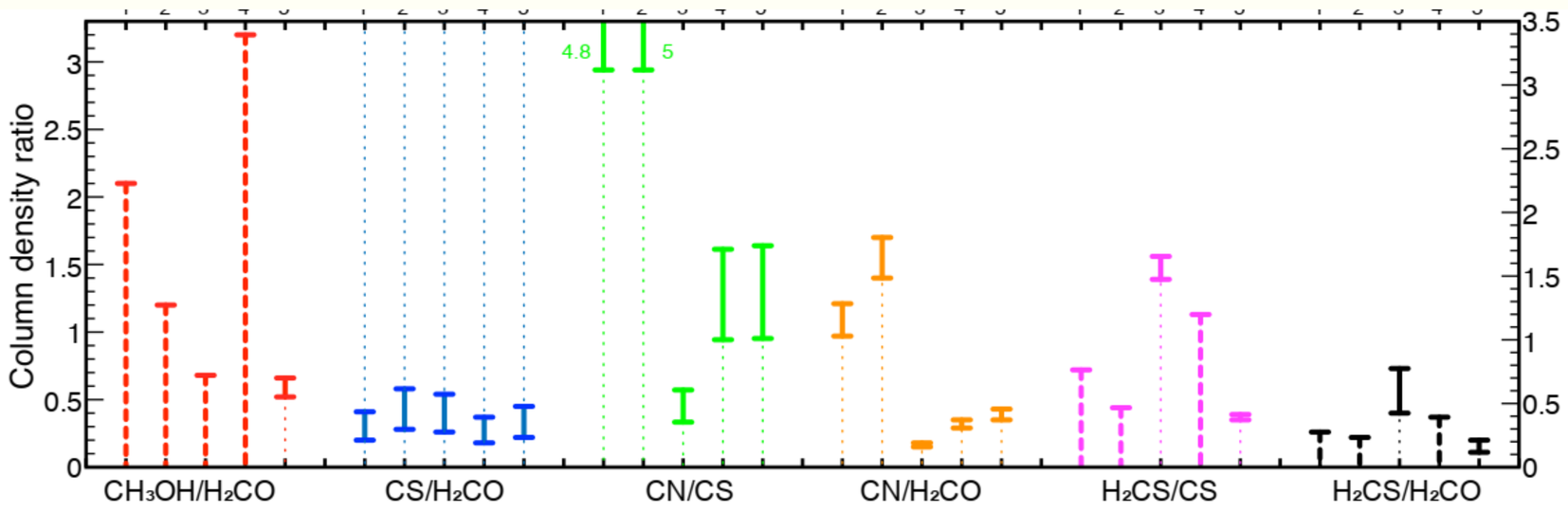

Fig. 7. Column density ratios. Continuous lines indicate the range of solutions found in the hypothesis of optically thin lines in the range of gas temperature 20−100 K. Dashed lines indicate upper limits from undetected lines. The possibility that CS and H_2CO lines are optically thick is reflected by the thin dotted lines. When a bar falls outside of the diagram, the upper limit is indicated. Sources are ordered as (1) DG Tau, (2) DG Tau B, (3) HL Tau, (4) Haro 6-13, and (5) IRAS04302.

#11 検出できなかった輝線

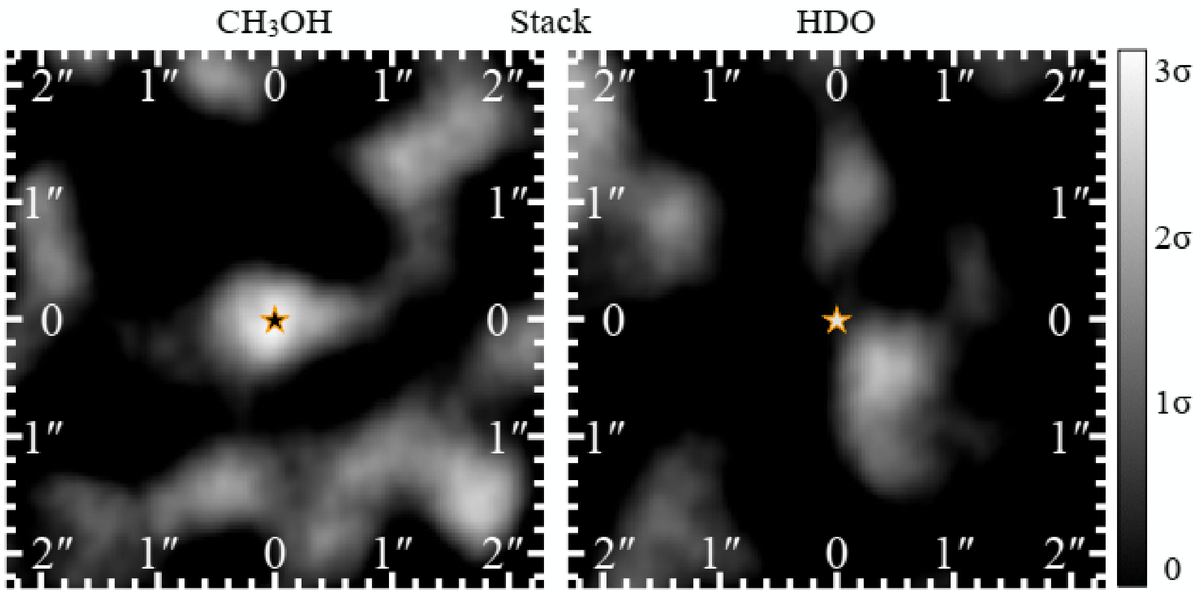

Fig. 8. Moment 0 maps of CH_3OH (left) and HDO (right) obtained by stacking maps of all sources with non-detections and smoothing by 1″.

個々の天体では未検出だった輝線CH3OH, HDOの観測結果をスタックしたもの
・CH3OHは2.5σのシグナル検出 (今後深い観測を行えば検出可能な値)
・HDOはスタックしてもシグナルは見られず

まとめ
・12COはアウトフロー・エンベロープ起源の信号が混ざってしまう
・CSとH2COはガス円盤のよいトレーサー (特にH2CO)
・CNはガス円盤のよいトレーサーとはならない。
・CH3OHは今後の観測によって検出される可能性がある

Chamaeleon DANCe. Revisiting the stellar populations of Chamaeleon I and Chamaeleon II with Gaia-DR2 data

P. A. B. Galli, H. Bouy, J. Olivares, N. Miret-Roig, L. M. Sarro, D. Barrado, A. Berihuete, E. Bertin, J. C. Cuillandre

Context: Chamaeleon is the southernmost low-mass star-forming complex within 200 pc from the Sun. Its stellar population has been extensively studied in the past, but the current census of the stellar content is not complete yet and deserves further investigation. Aims: We take advantage of the second data release of the *Gaia* space mission to expand the census of stars in Chamaeleon and to revisit the properties of the stellar populations associated to the Chamaeleon I (Cha I) and Chamaeleon II (Cha II) dark clouds. Methods: We perform a membership analysis of the sources in the *Gaia* catalogue over a field of 100 deg^2 encompassing the Chamaeleon clouds, and use this new census of cluster members to investigate the 6D structure of the complex. Results: We identify 188 and 41 high-probability members of the stellar populations in Cha I and Cha II, respectively, including 19 and 7 new members. Our sample covers the magnitude range from $G = 6$ to $G = 20$ mag in Cha I, and from $G = 12$ to $G = 18$ mag in Cha II. We confirm that the northern and southern subgroups of Cha I are located at different distances ($191.4^{+0.8}_{-0.8}$ pc and $186.7^{+1.0}_{-1.0}$ pc), but they exhibit the same space motion within the reported uncertainties. Cha II is located at a distance of $197.5^{+1.0}_{-0.9}$ pc and exhibits a space motion that is consistent with Cha I within the admittedly large uncertainties on the spatial velocities of the stars that come from radial velocity data. The median age of the stars derived from the Hertzsprung-Russell diagram (HRD) and stellar models is about 1-2 Myr, suggesting that they are somewhat younger than previously thought. We do not detect significant age differences between the Chamaeleon subgroups, but we show that Cha II exhibits a higher fraction of disc-bearing stars compared to Cha I.

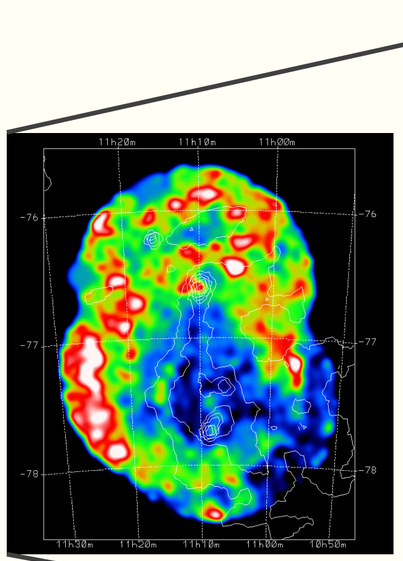

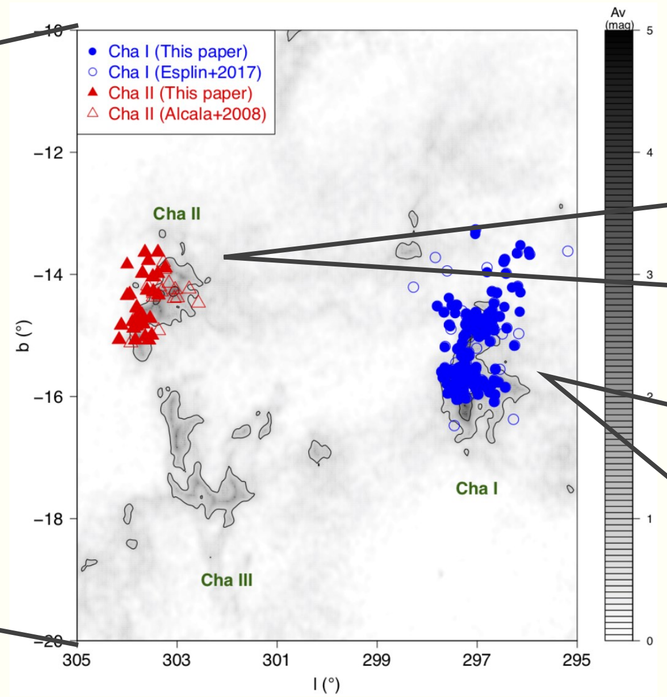

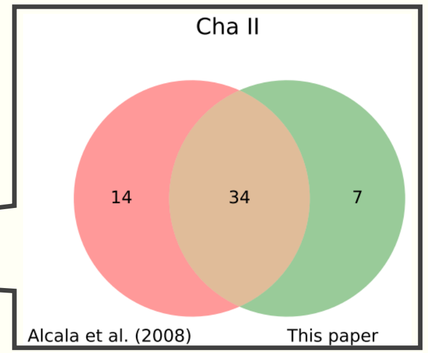

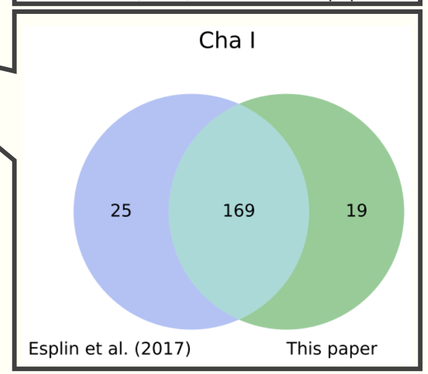

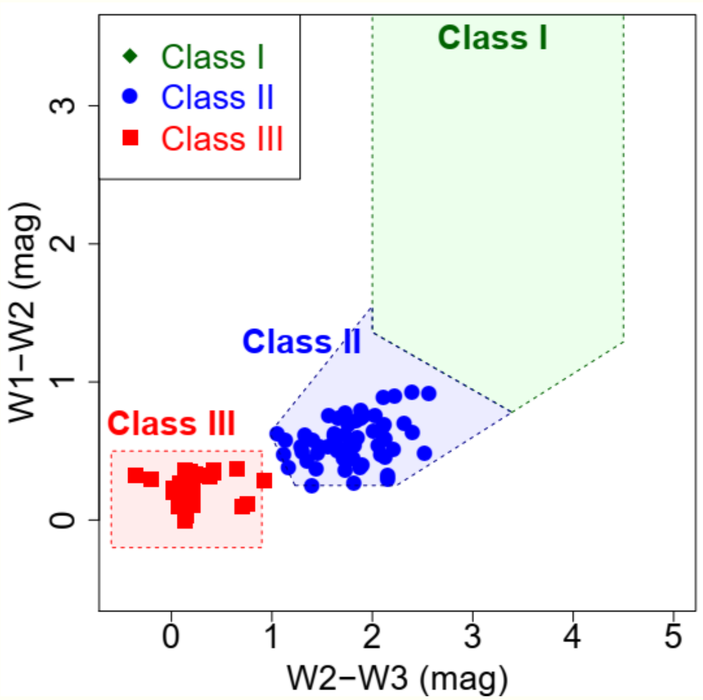

The Geometry and Dynamical Role of Stellar Wind Bubbles in Photoionised HII Regions

Sam Geen, Rebekka Bieri, Joakim Rosdahl, Alex de Koter

Winds from young massive stars contribute a large amount of energy to their host molecular clouds. This has consequences for the dynamics and observable structure of star-forming clouds. In this paper, we present radiative magnetohydrodynamic simulations of turbulent molecular clouds that form individual stars of 30, 60 and 120 solar masses emitting winds and ultraviolet radiation following realistic stellar evolution tracks. We find that winds contribute to the total radial momentum carried by the expanding nebula around the star at 10% of the level of photoionisation feedback, and have only a small effect on the radial expansion of the nebula. Radiation pressure is largely negligible in the systems studied here. The 3D geometry and evolution of wind bubbles is highly aspherical and chaotic, characterised by fast-moving "chimneys" and thermally-driven "plumes". These plumes can sometimes become disconnected from the stellar source due to dense gas flows in the cloud. Our results compare favourably with the findings of relevant simulations, analytic models and observations in the literature while demonstrating the need for full 3D simulations including stellar winds. However, more targeted simulations are needed to better understand results from observational studies.

Simulation name	Cloud	M_* / $M_\odot$	UV	WIND	PRESS
NOFB	DIFFUSE	-	✗	✗	✗
UV_30	DIFFUSE	30	✓	✗	✗
UVWIND_30	DIFFUSE	30	✓	✓	✗
UVWINDPRESS_30	DIFFUSE	30	✓	✓	✓
UV_60	DIFFUSE	60	✓	✗	✗
UVWIND_60	DIFFUSE	60	✓	✓	✗
UVWINDPRESS_60	DIFFUSE	60	✓	✓	✓
UV_120	DIFFUSE	120	✓	✗	✗
UVWIND_120	DIFFUSE	120	✓	✓	✗
UVWINDPRESS_120	DIFFUSE	120	✓	✓	✓
NOFB_DENSE	DENSE	-	✗	✗	✗
UV_120_DENSE	DENSE	120	✓	✗	✗
UVWIND_120_DENSE	DENSE	120	✓	✓	✗
UVWINDPRESS_120_DENSE	DENSE	120	✓	✓	✓

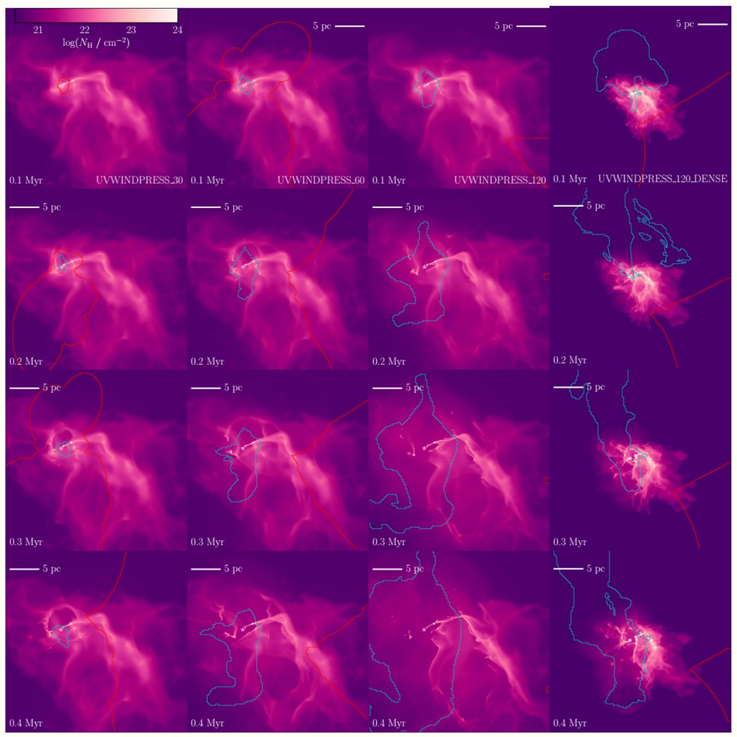

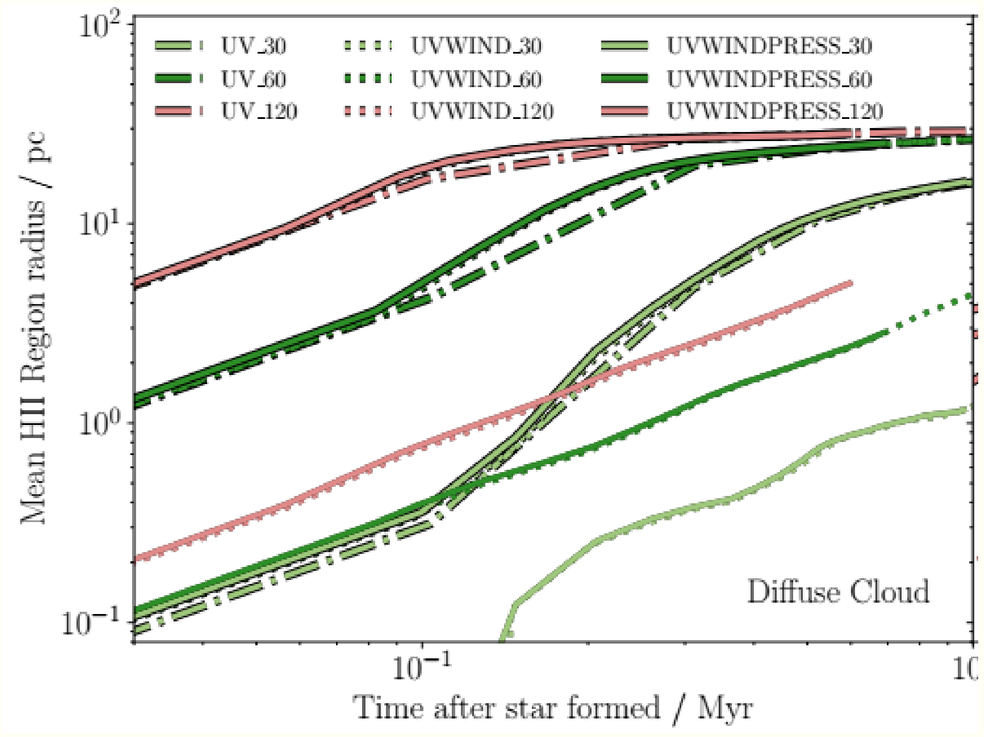

3D dynamics of the Orion cloud complex – Discovery of coherent radial gas motions at the 100-pc scale

Josefa E. Großschedl, João Alves, Stefan Meingast, Gabor Herbst-Kiss We present the first study of the 3D dynamics of the gas in the entire southern Orion cloud complex. We used the parallaxes and proper motions of YSOs from Gaia DR2 as a proxy for gas distance and proper motion, and the gas radial velocities from archival CO data, to compute the space motions of the different star-forming clouds in the complex, including subregions in Orion A, Orion B, and two outlying cometary clouds. From the analysis of the clouds' orbits in space and time, we find that they were closest about 6 Myr ago and are moving radially away from roughly the same region in space. This coherent 100-pc scale radial motion supports a scenario where the entire complex is reacting to a major feedback event, which we name the Orion-BB (big blast) event. This event, which we tentatively associate with the recently discovered Orion X stellar population, shaped the distribution and kinematics of the gas we observe today, although it is unlikely to have been the sole major feedback event in the region. We argue that the dynamics of most of the YSOs carry the memory of the feedback-driven star formation history in Orion and that the majority of the young stars in this complex are a product of large-scale triggering, which can raise the star formation rate by at least an order of magnitude, as for the head of Orion A (the Integral Shape Filament). Our results imply that a feedback, compression, and triggering process lies at the genesis of the Orion Nebula Cluster and NGC2023/2024 in Orion B, thus confirming broadly the classical feedback-driven scenario proposed in Elmegreen & Lada (1977). The space motions of the well-known young compact clusters, σ Orionis and NGC 1977, are consistent with this scenario. A momentum estimate suggests that the energy of a few to several supernovae is needed to power the coherent 3D gas motion we measure in this paper.

Label	Region	Subregion	N_{Gaia}
1	Orion A (tail)	L1647-S	17
2	Orion A (tail)	L1647-N	32
3	Orion A (tail)	L1641-S	69
4	Orion A (tail)	L1641-S/C	29
5	Orion A (tail)	L1641-C	70
6	Orion A (head)[a]	L1641-N	181
7	Orion A (head)	OMC-4/5	116
8	Orion A (head)	OMC-1	186
9	Orion A (head)	OMC-2/3	115
10	Orion B (main)	L1630-S	57
11	Orion B (main)	L1630-N	74
12	Orion B (cometary)	L1622	8
13	Outlying Cloud (cometary)	L1616	18
14	Outlying Cloud (cometary)	IC2118	5
15	Cluster[b]	Orion X	135

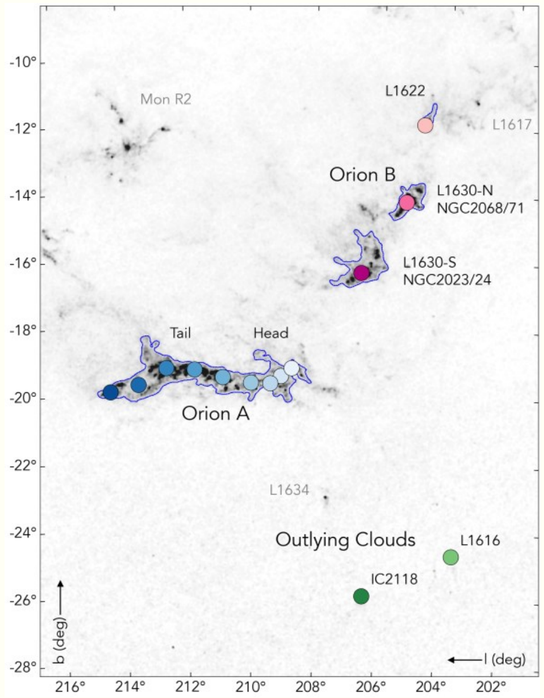

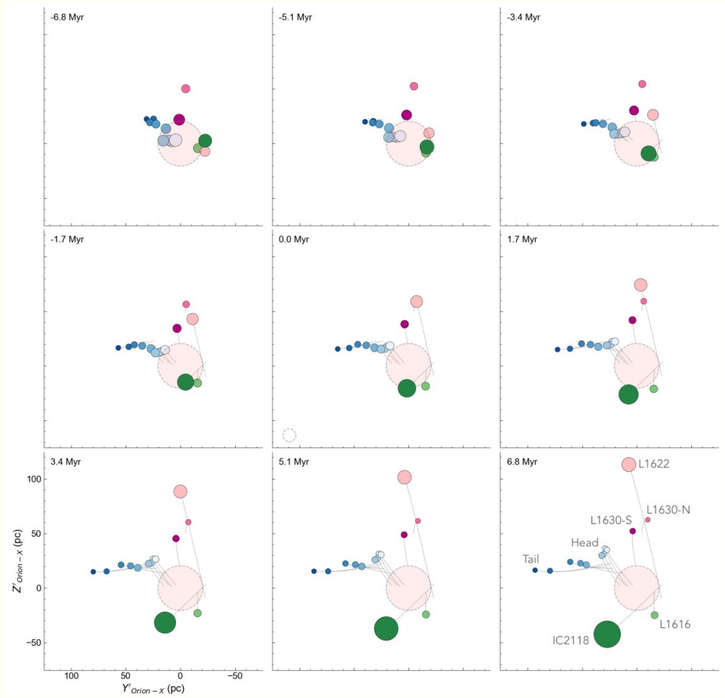

Simulating Star Clusters Across Cosmic Time: II. Escape Fraction of Ionizing Photons from Molecular Clouds

Chong-Chong He, Massimo Ricotti, Sam Geen We calculate the hydrogen and helium-ionizing radiation escaping star-forming molecular clouds, as a function of the star cluster mass and compactness, using a set of high-resolution radiation-magneto-hydrodynamic simulations of star formation in self-gravitating, turbulent molecular clouds. In these simulations, presented in He, Ricotti and Geen (2019), the formation of individual massive stars are well resolved, and their UV radiation feedback and lifetime on the main sequence are modeled self-consistently. We find that the escape fraction of ionizing radiation from molecular clouds, $\langle f_{\rm esc}^{\rm MC}\rangle$, decreases with increasing mass of the star cluster and with decreasing compactness. Molecular clouds with densities typically found in the local Universe have negligible $\langle f_{\rm esc}^{\rm MC}\rangle$, ranging between 0.5% to 5%. Ten times denser molecular clouds have $\langle f_{\rm esc}^{\rm MC}\rangle \approx 10\% - 20\%$, while 100× denser clouds, which produce globular cluster progenitors, have $\langle f_{\rm esc}^{\rm MC}\rangle \approx 20\% - 60\%$. We find that $\langle f_{\rm esc}^{\rm MC}\rangle$ increases with decreasing gas metallicity, even when ignoring dust extinction, due to stronger radiation feedback. However, the total number of escaping ionizing photons decreases with decreasing metallicity because the star formation efficiency is reduced. We conclude that the sources of reionization at $z > 6$ must have been very compact star clusters forming in molecular clouds about 100× denser than in today's Universe, which leads to a significant production of old globular clusters progenitors.

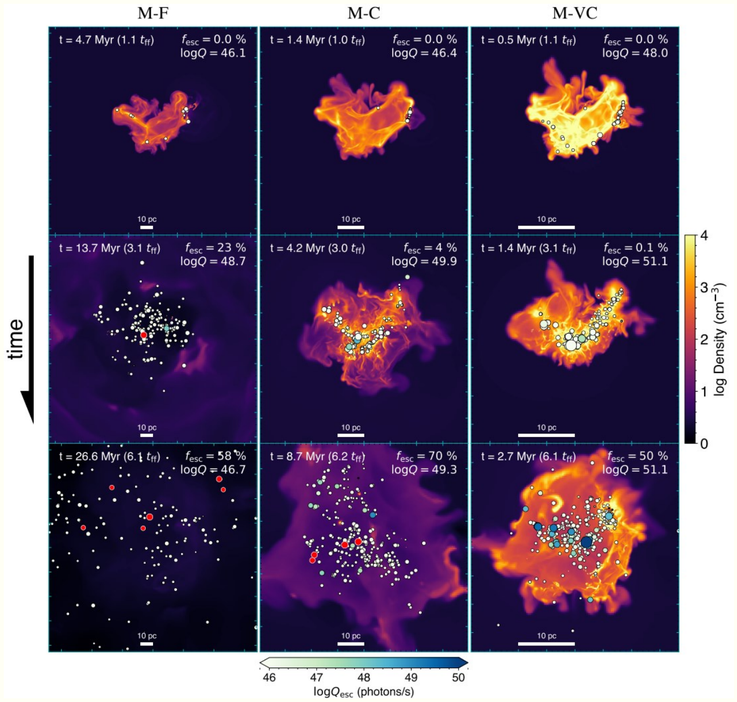

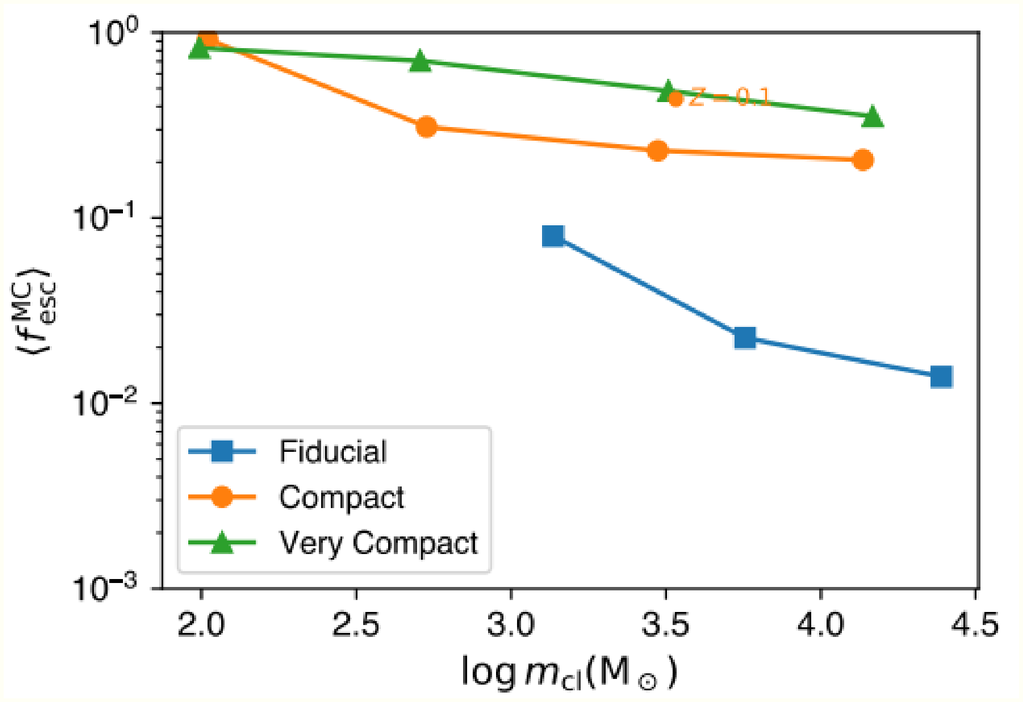

#15「大質量YSOアウトバーストでの水メーザー変動」

Water maser variability in a high-mass YSO outburst – VERA and ALMA observations of S255 NIRS 3

Tomoya Hirota, Riccardo Cesaroni, Luca Moscadelli, Koichiro Sugiyama, Ross A. Burns, Jungha Kim, Kazuyoshi Sunada, Yoshinori Yonekura We carried out observations of the 22 GHz H2O masers in a high-mass protostar S255 NIRS 3 by using VERA. We measured the proper motions of the 22 GHz H2O masers associated with a bipolar outflow. The expansion velocity of the blueshifted bow shock traced by the 22 GHz H2O masers was 28 km s-1 corresponding to a dynamical timescale of 60 years. The direction of the maser outflow is slightly tilted compared with the radio jet, which could suggest a more recent ejection episode during the accretion burst event. The total flux density of the 22 GHz H2O masers has gradually increased from early 2017 and has become almost constant in 2018. For the first time, we reveal extended H2O maser emission at 22 GHz in a star forming region, which is partly resolved out by VERA and even by the most extended VLA configurations. We find that the flux variation of such an extended component is similar to that of the unresolved maser emission. We also conducted observations of the submillimeter continuum and the 321 GHz H2O masers with ALMA at Band 7. The continuum emission does not show significant variations compared with the previous observations performed 5 months before. We mapped the 321 GHz H2O masers in S255 NIRS 3 providing the fourth example, for this maser, of the spatial distribution in a high-mass star-forming region. The lower ratio of the 22 GHz/321 GHz maser luminosity in the blueshifted bow shock suggests a temperature (>1000 K), higher than for the other maser features in this region. We conclude that the bow shock structure traced by the 22 GHz H2O maser features is unlikely to be originating at the interface between the radio jet powered by the recent accretion outburst and the surrounding medium. The brightening of the 22 GHz H2O masers could be due to radiative excitation by photons form the infrared outburst escaping along the cavity created by the newly ejected material.